Driving forces for particle-based crystallization: From experiments to theory and simulations

Maria L. Sushko*

The multistep crystallization processes involving the formation of stable building blocks that subsequently assemble into a crystal are ubiquitous in mineral formation and biomineralization and are particularly attractive in materials synthesis. Utilizing these pathways offers the approach to overcoming the restrictions on the expression of various crystal faces imposed by the interfacial energy during monomer-by-monomer growth to unlock the breadth of architectures with unique properties. Controlling particle-based crystallization proved challenging despite its promise due to the complex interdependence of interfacial forces and their nonlinear dependence on synthesis parameters. Here, the status of the development of state-of-the-art approaches to measuring interparticle forces and predictive theoretical models of particle-based crystallization are reviewed.

Introduction

Among nonclassical crystallization pathways, particle-based crystallization is particularly interesting because it provides unique insights into interfacial forces and their effect on subsequent nucleation and growth processes. The first step in the particle-based crystallization pathway constitutes the formation of multi-monomer precursors, such as droplets,[1–3] clusters,[4–7] and amorphous[8–15] or crystalline[16,17] nanoparticles, which subsequently undergo transformation and assembly into crystalline structures as evidenced by *in situ* observations (**Figure 1**a). Creating mineral surfaces during the nucleation step results in symmetry breaking in precursor solution and introduces several interfacial forces that direct subsequent growth.[18–20] Interfacial speciation is profoundly affected by the details of nanoparticle structure and charge distribution resulting in the formation of the electric double layer around the nucleated nanoparticles. The interactions within the electric double layer, in turn, mediate interparticle forces and direct their subsequent assembly via either oriented attachment (OA) to produce single crystals or twinned nanostructures, or coalescence through misoriented assembly. Each pathway can be uniquely characterized by the shape of the interparticle force curve that reflects the interplay of enthalpic and entropic interactions between the opposing electric double layers and macroscopic interparticle forces (Figure 1b).

The discovery that nucleation and growth are not necessarily separate processes, but could be happening simultaneously,[21,22] further complicated the prediction of the outcomes of particle-based crystallization. The link between the creation of the interface and nucleation in the interfacial region points to the insufficiency of the considerations of interparticle forces and highlights the requirements to complement these findings with the prediction of the forces acting on precursor species in the interfacial region of each particle. The advances in the development of such a nuanced framework for understanding and predicting the pathways involving initial symmetry breaking due to the formation of first crystalline or amorphous nanoparticles is the topic of this review.

Particle stability and growth pathways

Before discussing particle dynamics during particle-based crystallization, it is instructive to determine how the interactions in precursor solution at the particle surface affect its stability. Coupled with *in situ* transmission electron microscopy (TEM), atomic force microscopy (AFM) studies and atomistic-to-mesoscopic simulations revealed that the potential of mean force of

Maria L. Sushko, Physical Sciences Division, Pacific Northwest National Laboratory, Richland, USA; maria.sushko@pnnl.gov
doi:10.1557/s43577-024-00696-8

© Battelle Memorial Institute, USA 2024

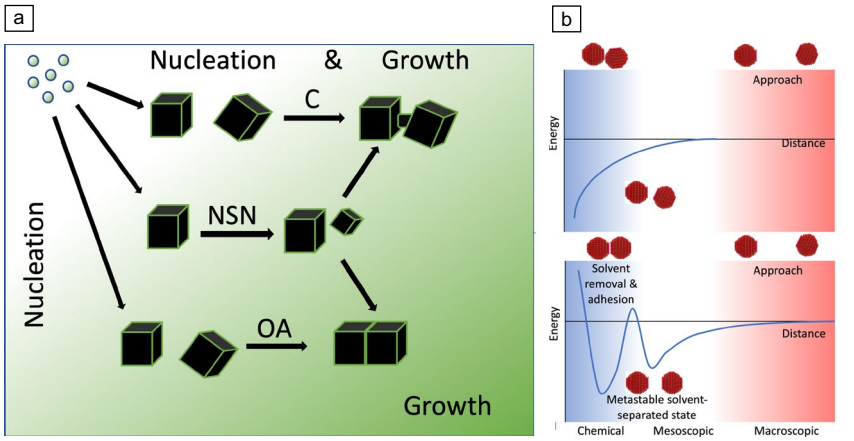

Figure 1. Particle-based crystallization pathways and characteristic interparticle force curves. (a) A subset of pathways discussed here includes coalescence (C), near-surface nucleation (NSN), and oriented attachment (OA). (b) The characteristic force curves for coalescence are monotonically attractive. In contrast, the force curve for two particles undergoing OA has at least two minima: the minimum at larger separations marks the metastable state, which promotes fine alignment of nanoparticles before attachment.

precursor species is a descriptor for particle stability and growth pathway. Specifically, by separating the contributions to the total chemical potential of precursor ions into the entropy of mixing (ideal chemical potential) and the terms containing all interfacial interactions (potential of mean force—PMF), it becomes feasible to predict the driving forces and barriers for precursor deposition.[23,24] The PMF with a minimum at the interface and attractive short-range precursor/surface interactions favors classical monomer addition. Repulsive PMFs indicating that the surface is stable are often due to precursor species forming a highly correlated double layer at the interface. Repulsive PMFs are the prerequisite for particle-based crystallization or the formation of stable emulsion. The intermediate scenario was discovered in the presence of charged ligands. Similar to repulsive PMF, the potential of mean force is dominated by entropic ion correlation interactions. However, instead of being purely repulsive, the PMF has a minimum at approximately a nanometer separation from the surface, promoting nucleation in the interfacial region of the parent particle.[21,22] The following discussion will focus on the details of interparticle forces under the conditions with repulsive PMF for precursor species at separations below a nanometer from the nanoparticle surfaces, which exclude classical growth by monomer addition.

Mechanism of oriented attachment

The oriented attachment (OA) process furnishes an ideal platform for the development of a detailed understanding of interparticle forces beyond the confines of classical colloidal theory. Intrinsic face selectivity during the OA necessarily requires considering the atomistic structure of nanoparticle faces and of the interfacial electrolyte forming the electric double layer. The complex dynamics of nanoparticles undergoing multiple rotations and translations during the oriented attachment process as revealed by *in situ* observation often points to the qualitative changes in particle motion at different stages of the approach.[19,25–27] It is instructive, therefore, to divide the OA dynamics into the following four stages characterized by different dominating forces driving face selectivity and alignment.

Approach

The long-range character of interparticle attractive forces was demonstrated using liquid-cell TEM.[23,28,29] The directionality and face specificity of particle motion were detected at separations as high as tens of nanometers indicating that macroscopic interparticle forces can drive the initial approach. The dominating forces between the particles at separations larger than their diameters encompass spontaneous dipolar polarization, interparticle van der Waals forces, and mesoscopic van der Waals interactions caused by correlated fluctuations of ionic densities within the electric double layer (i.e., ion correlation forces). The strength of directional van der Waals, dipolar, and ion correlation forces increases as particles move closer together, causing a decrease in the relative impact of stochastic hydrodynamic drag. As the distance between the particles decreases, their drift velocity increases.

Capture minimum

When particle separation becomes commensurate with their radii, face-specific ion correlation, and interparticle van der Waals forces can become stronger than electrostatic forces, resulting in a net force minimum for specific surfaces and conditions. This attraction becomes stronger with an increase in surface charge density and valency of the counterions,[30] which explains the experimentally observed sensitivity of the OA process to bulk solvent properties, such as pH, electrolyte concentration, and chemistry.[29,31–34] This ion correlation torque between specific particle faces can rotate misaligned particles into a lattice-matching orientation. Weaker hydration and ion–surface interactions can cause specific ion effects by altering ion distribution and influencing ion correlation force.

Adhesion barrier

The approach to the distance of three to six layers of solvent marks the onset of the repulsive regime. The barrier is mainly due to the repulsion between the opposing layers of adsorbed counterions and steric hydration. These forces cause a shift in the outer Helmholtz plane of the electrical double layer, leading to a monotonic repulsion between the particles.[27] When

nanoparticle separation decreases to one to three solvent layers, the energy gained to hydrate ions in the gap between nanoparticles drives water into this region. To accommodate a high concentration of water between nanoparticles as dictated by ion and surface hydration, a loss in water entropy occurs through enhanced structuring and depolarization. This leads to the creation of an osmotic repulsive force, pushing the faces apart.[35,36] These forces arise from the structure and properties of the confined solvent, creating an energy barrier that maintains particle separation beyond the range of chemical forces.[37]

Adhesion

When two surfaces with aligned or nearly aligned lattices come into contact, corresponding to the primary minimum of the particle–particle interaction force curve, adhesion occurs. This process is driven by chemical forces such as hydrogen bonding and interatomic van der Waals forces. It has been proposed that the removal of a crystal facet with high surface energy reduces the total surface energy and drives OA.[38] It is important to note that crystal faces with higher vacuum surface energy are more reactive to solution species, which affects interparticle forces and modifies their surface energy. Thereby, the surface energy of crystal faces in vacuum could correlate with the probability of OA, but this correlation is not absolute in the absence of macroscopic material anisotropy.

The adhesion process encompasses solvent exclusion, defect elimination, and lattice fusion.[29] In the absence of direct experimental observations probing the mechanism of solvent exclusion, molecular simulations were used to understand the dynamics of the last few layers of confined water. The expulsion of ions is likely to precede the expulsion of the last two layers of water because it is energetically favorable for ions to restore their full hydration shell and gain entropy by diffusing into the bulk solution.[39,40] Though indirectly, this theoretical prediction is corroborated by the experimental observations of the independence of hydration repulsion at short separations on the nature and concentration of electrolytes.[35] At the final stage, it is also necessary to remove any dissociated water that could have adsorbed on particle surfaces during the final stages of adhesion. In a case study, molecular dynamics analysis predicted that hydroxyls of dissociated water recombine with protons in TiO_2, leaving a gap in a zipper-like fashion.[25,26] Eventually, a gradual process of removing defects occurs.

The initial focus of the quest to understand the origin of long-range face selectivity during the OA was to evaluate whether macroscopic colloidal interactions across a mean-field medium could provide a reliable model of the OA mechanism. Experimental studies were conducted to separate different types of interactions and verify the accuracy of macroscopic theories. These theories consider the face specificity of bulk properties of nanocrystals, such as the anisotropy in their static and dynamic dispersion responses, dipolar polarization, and the distribution of surface charge.

The anisotropy of van der Waals interactions between nanocrystals can have three origins. The first is the intrinsic anisotropy of the dielectric response of the corresponding bulk material. The second is the shape anisotropy of the particles. Finally, it can be a combination of both of these effects.[41,42] The range of van der Waals torque due to shape anisotropy is typically commensurate with the particle size.[41] An experimental method was developed to test the effect of orientation dependence on a material's dielectric response. This method integrated an atomic force microscopy probe with environmental transmission electron microscopy (TEM) to measure the force–distance relationships between two single crystals while directly imaging the interparticle gap (**Figure 2**).[43] The experiments were conducted in high-vacuum conditions and in the presence of water vapor to isolate interparticle van der Waals interactions as the only significant attractive force between rutile TiO_2 nanocrystals. Quantitative agreement was demonstrated between the angular dependence of interparticle forces and the predictions of Lifshitz

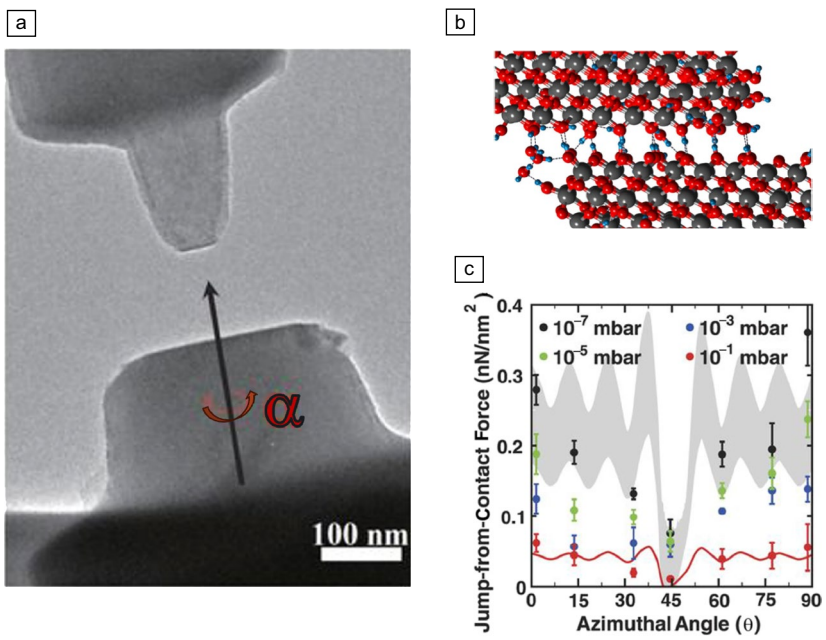

Figure 2. Revealing the origin of macroscopic and microscopic torque between nanocrystals. (a) Coupled atomic force microscopy/transmission electron microscopy measurements of the angular dependence of vdW torque between TiO_2 surfaces.[42] (b) Hydrogen bonding network. Reprinted with permission from References 26 and 42. © 2017 AAAS. (c) Measured (symbols) and calculated (lines) forces at various water pressures.

quantum electrodynamic theory of dispersion interactions. This study revealed that the van der Waals torque has a short-range nature and becomes negligible beyond 1.0–1.5 nm separations. When surfaces are approximately one hydration layer apart, the attraction is strongly dependent on azimuthal alignment and systematically decreases as intervening water density increases. These findings suggest that van der Waals torque between nanocrystals that are dielectrically anisotropic will contribute to their alignment during the adhesion stage when several layers of solvent separate particles.

Further studies investigated the behavior of nanocrystals in an isotropic solution by considering the coupling of van der Waals interactions and hydrodynamic effects.[44] The simulations predicted the alignment of nanocrystals along their optical axes in cubic and spherical optically anisotropic crystals. These results show that elongated nanocrystals can be aligned during the approach stage of OA by shape-specific van der Waals interactions. During the second stage of OA when several layers of solvent separate particles, van der Waals torque resulting from the material's optical anisotropy can aid in particle azimuthal alignment.

Electrostatic dipolar forces are typically long-range and directional and, therefore, were considered as one of the driving forces for the OA.[28] For nanoparticles with intrinsically anisotropic dipolar polarization, such as $BaTiO_3$, the changes in the directionality of the leading forces with particle size are due to the different scaling of the strength of van der Waals and dipolar interactions.[44] Residual spontaneous dipolar polarization can also play a role in interparticle interactions that depend on the orientation of the particles. The nature of dipolar forces can be twofold: (1) the material can have a permanent dipole along a certain crystallographic direction and is associated with the anisotropy in dipolar polarizability of the material, or (2) the particles can have a surface dipole on polar surfaces. The surface dipole, however, is often efficiently compensating in solution by partial hydroxylation or protonation of polar surfaces.[45–53] Due to the dynamic nature of water dissociation at surfaces, complete dipole compensation may not be achieved.[54] Therefore, residual spontaneous dipolar polarization can play a significant role in directional interparticle interactions under nonequilibrium conditions.[23,55]

Entropic and enthalpic hydration forces. Experimental evidence has documented the structuring of interfacial water that extends over several layers and is manifested in periodic density variations.[56,57] When two surfaces approach close enough for these structured water layers to overlap, they begin to experience entropic repulsion. Solvent structuring and the corresponding entropic hydration forces oscillate with the number of water layers separating nanoparticles. The position and the height of the first density peak define the face specificity of the corresponding hydration forces. The sensitivity to particle alignment also stems from the dependence of water arrangement in the interfacial hydration layer as predicted by molecular dynamics simulations and measured using atomic force microscopy.[57,58] For example, force measurements and molecular simulations revealed a 60º periodicity in the forces acting between two ZnO faces in an aqueous solution.[37]

A reactive molecular dynamics approach was used to analyze the role of face-specific enthalpic hydration interactions in detail.[26] The simulations showed that when there is no water present, the anatase TiO_2 nanocrystals interact without any specific direction or orientation. Instead, they attach along the path of their approach, which indicates that their aggregation is driven by the isotropic van der Waals forces. Water vapor alters the short-range interactions between particles. The adsorbed water molecules create a dynamic network of hydrogen bonds between the nanocrystals, promoting their alignment (Figure 2). The propensity of various crystal faces to dissociate water also plays a commanding role, and the alignment of particles at separations below 0.3 nm is mainly driven by electrostatic interactions between adsorbed hydroxyl groups. These studies emphasize the importance of interfacial water structure, dynamics, and reactivity in nanocrystal face selectivity and alignment.

Face-specific forces in electrolyte solutions. The unique properties of solvent and ions in electrolytes cause ion-specific forces that drive the OA process between particles.[59] These effects have an intrinsically atomistic nature and cannot be captured by mean-field theories. For example, by changing the counterion from bromide to acetate, forces can vary by more than an order of magnitude.[60–62] These ion-specific effects suggest that ion solvation and ion fluctuation dynamics play a crucial role in directing the OA. Experimental studies have demonstrated that the pathway of nanoparticle assembly ranging from OA to random aggregation is significantly influenced by the properties of aqueous electrolyte solutions. Even small variations in the ionic strength or pH of the solution can disrupt the mode of nanoparticle assembly.[31,32,63,64] The "quantization" of the adhesion forces between two surfaces was demonstrated both in electrolyte and in pure water using surface force apparatus measurements. These measurements revealed sharp adhesion energy peaks for the angular dependence of forces between two atomically flat mica surfaces.[65,66] In pure water, the surfaces immediately settle into the primary energy minimum. However, in the presence of 0.7 mM KCl, the surfaces first come to rest in a second, metastable, adhesive minimum where the adhesive force is about 25% of that in the primary minimum. After remaining in this solvent-separated state for several seconds, a jump-to-contact is observed. This dynamics of adhesion in the electrolyte solution is characteristic of particle dynamics during OA. The onset of a metastable solvent-separated state is essential for particle alignment in a lattice-matching orientation. A metastable state in an electrolyte solution cannot be driven solely by oscillatory entropic hydration forces. Ion distributions and dynamics in the EDL at nanocrystal-solution interfaces play a unique role in creating both osmotic pressure and azimuthal torque between lattice-mismatched crystal surfaces.[27,67]

Interactions in the opposing EDLs that drive face selectivity vary in range from short-range pairwise chemical forces

to long-range many-body interactions. The common feature of these forces is their dependence on the atomic structure and the discrete charge distribution on nanoparticle faces. Thereby, face selectivity is an intrinsic property of electrolyte-mediated interactions, which often compete with nonspecific van der Waals interactions between particles. Short-range forces encompass dispersion ion–surface interactions and chemical bonding of partially desolvated ions, if any, to the surface sites. In contrast, interactions in and between the opposing EDLs have a many-body nature. These mesoscale interactions do not depend on the position and velocity of each individual ion or solvent molecule. Instead, collective fluctuation dynamics of ions in the EDL introduce charge-density fluctuations. The resulting fluctuating dipoles induce a mesoscale dipolar response in the opposing EDL. These forces known as ion correlation forces can, therefore, be viewed as a mesoscale analogue to interatomic van der Waals interactions. Ion correlation forces are ion-specific because they depend not only on ion charge and size but also on its polarizability and solvation. Furthermore, these interactions are sensitive to the arrangement of charged species on the nanoparticle surface, pH, and concentration of electrolyte providing a direct link between experimental solution composition and the strength of interparticle forces.[23,40,64] In many cases, these interactions lead to long- to medium-range attraction between like-charged surfaces[67,68] and polyelectrolytes[69] even in low salt conditions.

When driven by ion correlation interactions, OA was shown to be a statistically deterministic process that does not depend on crystal habit.[24] It has been revealed using *in situ* and high-resolution TEM that the directionality of attachment depends exclusively on the structure of solvated crystal faces. The mechanism of OA of hematite nanoparticles along specific crystal faces regardless of particle morphology is derived from the analysis of interparticle forces between the pairs of hematite surfaces (**Figure 3**). For all pairs of crystal faces, these interactions are dominated by ion correlation forces, which create a prohibitively high barrier at separations of 1–2 nm between all faces except (001). This strict directionality of attractive interparticle forces is dictated by the response of correlated dynamics in the EDL to the distribution of surface charges due to the dissociative adsorption of water at hematite faces. The generality of the conclusion is supported by the studies of OA between anatase TiO_2 nanoparticles controlled by solution pH.[40] Similarly, directional attractive interactions between particle faces are observed only in the narrow pH range that produces a hexagonal array of surface charges on (112) anatase faces.

The strength and range of ion correlation interactions for hematite, anatase TiO_2, and ZnO nanoparticles are closely correlated with the configuration of charged groups on the crystal face, indicating that the configuration of charged groups on different crystal faces could be used to predict the most likely direction of OA. Such charged entities are typically obtained

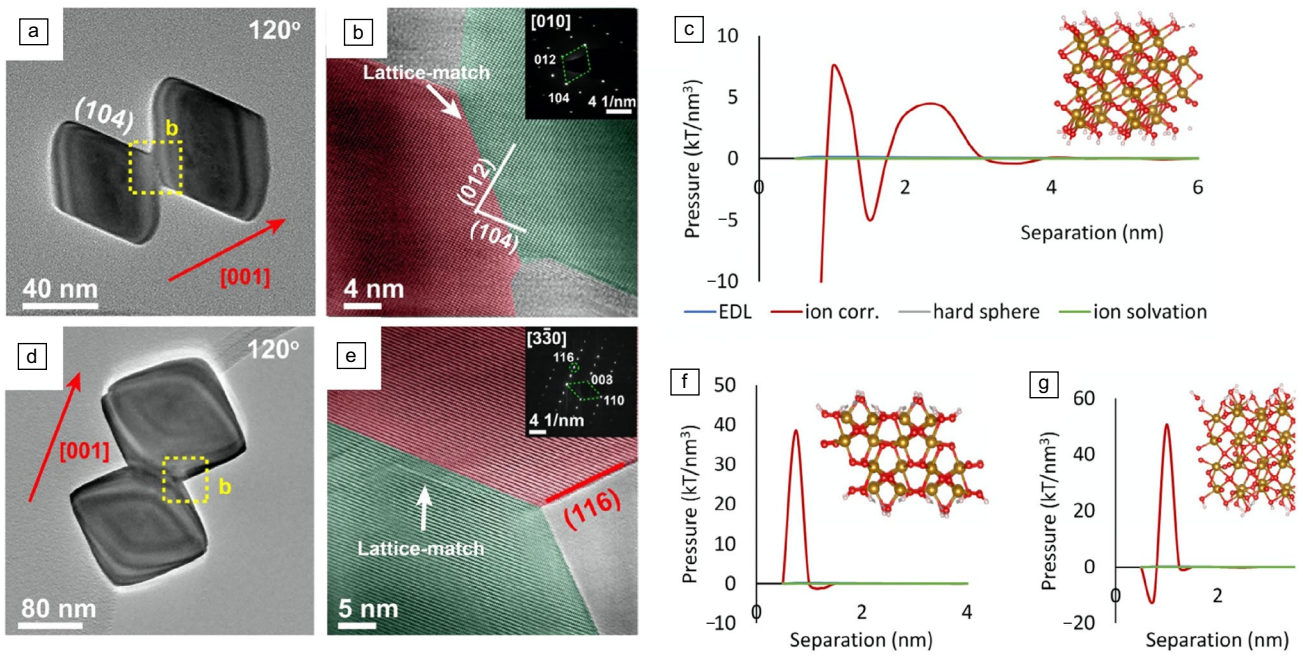

Figure 3. Driving forces for the formation of 1D arrays of hematite nanocrystals. The arrays of rhombic nanoparticles with 6 {104} facets (a, b) and hexagonal bipyramidal nanoparticles with 12 {116} facets (d, e) are formed by oriented attachment. (a, d) Low-magnification transmission electron microscopy (TEM) image of aggregated hematite dimers and (b, e) high-resolution TEM image of lattice-matched particles boundary. Interactions between (c) two {001}, (f) two {012}, and (g) two {104} hematite faces. Insets in (c, f, g) show the structure of hydroxylated hematite faces. EDL, electric double layer. Adapted with permission from Reference 24. © 2022 National Academy of Sciences.

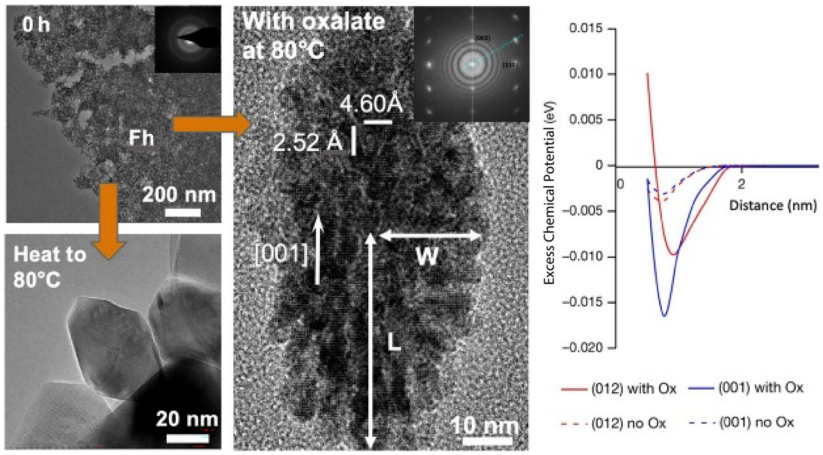

Figure 4. Coupled nucleation and oriented attachment pathway for the formation of spindle-shaped hematite mesocrystals. Transmission electron microscopy images show the structure of ferrihydrite (Fh, top left), initial hematite seeds with smooth surface (bottom left), and hematite spindle (middle). Average potential of mean force of Fe ions at hematite (001) and (012) surfaces, with (solid lines) and without (dashed lines) Ox (right). Adapted with permission from Reference 22. © 2021 Springer Nature.

for oxides in aqueous solutions by water dissociation and partial protonation or hydroxylation of the surfaces. Then, the pH and electrolyte concentration, along with the surface atomic ordering, determine the distribution of discrete charges on the surface. Alternatively, targeted surface functionalization can be used to generate a desired distribution of charged species on particular crystal faces. This method, which is frequently and effectively applied in the synthesis of materials, involves the assembly of ordered nanostructures through the OA of functionalized nanocrystals.[18,70,71] After achieving the correct surface chemistry, the electrolyte's characteristics, such as the ions' size, charge, and solvation state, can be chosen to further fine-tune the interparticle interactions.

Coupled near-surface nucleation and assembly

The formation of nanostructured architecture via a particle-based crystallization pathway often involves independent nucleation events followed by particle assembly. However, it was discovered that nucleation and growth processes are not always independent because initial nucleation events can sufficiently modify the solution structure in the interfacial region of the growing nucleus to promote further nucleation in this region. The coupling between particle-based growth and interfacial nucleation requires a barrier preventing direct monomer deposition onto the parent particle, which can be achieved by using charged ligands. The pathway was first identified in a model system of gold salt in an aqueous solution containing citrate.[21] The seeded growth experiments revealed that nucleation is confined to a narrow interfacial region of seed particles. Following nucleation, new particles either undergo a diffusive jump and attach to a seed particle or remain in the solvent-separated state closing the gap through the growth of a neck between the seed and the new particle. The aggregates did not have any specific mutual orientation because coalescence was driven by the isotropic van der Waals forces.

These studies also revealed that coalescence is not always a single-step process involving diffusive jump-to-contact. Instead, a two-step coupled diffusion and nucleation could occur. A detailed study of the dynamics of gold particles undergoing coalescence revealed that even nonspecific aggregation can be a two-step process. *In situ* studies of gold particle dynamics showed that hydration barrier at short separations can cause particles to dwell about 0.5 nm apart.[72–77] Instead of undergoing the diffusive jump-to-contact, nanoparticles in the precursor solution remain separated by two hydration layers. The confinement and the hydrophobic nature of gold cations promote cation accumulation in the gap, displacement of hydration water, and the nucleation of the amorphous bridge between the particles.[78]

The ubiquitous nature of coupled nucleation and growth pathway was further confirmed using a model of ligand-assisted crystallization of metal oxide.[22] The study demonstrated the formation of mesocrystals via interface-driven nucleation and growth, followed by OA (**Figure 4**). Hematite mesocrystals formation through ferrihydrite nanoparticle dissolution and recrystallization was observed in the presence of oxalate (Ox). In this process, the first hematite particles formed in close association with ferrihydrite. Subsequent crystallization involves the nucleation of nanoparticles exclusively in the interfacial region of the parent particle driven by interfacial gradients in the EDL of the oxalate-decorated hematite surface. The crystal habit of the newly nucleated particles was also controlled by the adsorbed Ox ligands resulting in the growth of self-similar morphology. Upon reaching the critical size, new particles undergo OA to form hematite spindles.

Conclusions

In recent years, significant progress has been achieved in our understanding of the mesoscopic and macroscopic forces that govern nonclassical crystallization in solution with major discoveries driven by the quest for the understanding of interfacial forces underpinning the OA process. Among the most important breakthroughs are the *in situ* observations of particle dynamics during OA and coalescence, the identification of the coupling between interface-controlled nucleation and growth during particle-based crystallization, and the development of a predictive theoretical framework that encompasses the details of the structure and forces in the EDL. But there are still a lot

of unanswered questions. For instance, we do not know if charge equilibration mechanisms involving hydroxylation, ion adsorption, and protonation/deprotonation alter surface charge density during particle approach, or how ions and solvents are removed from gaps between particles during jump-to-contact. Understanding these phenomena requires the development of new experimental methods with sufficient spatial and temporal resolution to capture interfacial dynamics at a molecular scale, while theoretical approaches must be extended to simultaneously capture dynamic molecular polarization interactions and the collective fluctuation dynamics in the EDL.

Acknowledgments

The work was supported by the US Department of Energy (DOE) Office of Science, Office of Basic Energy Sciences, Materials Sciences, and Engineering through its Synthesis & Processing Program FWP 12152 at Pacific Northwest National Laboratory, which is a DOE multiprogram national laboratory located in Richland, Wash.

Funding

Basic Energy Sciences, FWP12152, Maria Sushko.

Data availability

Not applicable.

Conflict of interest

The corresponding author states that there is no conflict of interest.

References

1. L.B. Gower, D.J. Odom, *J. Cryst. Growth* **210**, 719 (2000)
2. O. Galkin, K. Chen, R.L. Nagel, R.E. Hirsch, P.G. Vekilov, *Proc. Natl. Acad. Sci. U.S.A.* **99**, 8479 (2002)
3. M.A. Bewernitz, D. Gebauer, J. Long, H. Cölfen, L.B. Gower, *Faraday Discuss.* **159**, 291 (2012)
4. W.J.E.M. Habraken, J.H. Tao, L.J. Brylka, H. Friedrich, L. Bertinetti, A.S. Schenk, A. Verch, V. Dmitrovic, P.H.H. Bomans, P.M. Frederik, J. Laven, P. van der Schoot, B. Aichmayer, G. de With, J.J. De Yoreo, N.A.J.M. Sommerdijk, *Nat. Commun.* **4**, 1507 (2013)
5. A.I. Lupulescu, J.D. Rimer, *Science* **344**, 729 (2014)
6. A. Dey, P.H.H. Bomans, F.A. Müller, J. Will, P.M. Frederik, G. de With, N.A.J.M. Sommerdijk, *Nat. Mater.* **9**, 1010 (2010)
7. T.M. Davis, T.O. Drews, H. Ramanan, C. He, J.S. Dong, H. Schnablegger, M.A. Katsoulakis, E. Kokkoli, A.V. McCormick, R.L. Penn, M. Tsapatsis, *Nat. Mater.* **5**, 400 (2006)
8. E. Beniash, J. Aizenberg, L. Addadi, S. Weiner, *Proc. R. Soc. B-Biol. Sci.* **264**(1380), 461 (1997)
9. Y. Politi, T. Arad, E. Klein, S. Weiner, L. Addadi, *Science* **306**, 1161 (2004)
10. E. Beniash, R.A. Metzler, R.S.K. Lam, P.U.P.A. Gilbert, *J. Struct. Biol.* **166**, 133 (2009)
11. J. Mahamid, A. Sharir, L. Addadi, S. Weiner, *Proc. Natl. Acad. Sci. U.S.A.* **105**, 12748 (2008)
12. I.M. Weiss, N. Tuross, L. Addadi, S. Weiner, *J. Exp. Zool.* **293**, 478 (2002)
13. T.Y.J. Han, J. Aizenberg, *Chem. Mater.* **20**, 1064 (2008)
14. Y. Politi, R.A. Metzler, M. Abrecht, B. Gilbert, F.H. Wilt, I. Sagi, L. Addadi, S. Weiner, P.U.P.A. Gilbert, *Proc. Natl. Acad. Sci. U.S.A.* **105**, 17362 (2008)
15. A.V. Radha, T.Z. Forbes, C.E. Killian, P.U.P.A. Gilbert, A. Navrotsky, *Proc. Natl. Acad. Sci. U.S.A.* **107**, 16438 (2010)
16. J. Baumgartner, A. Dey, P.H.H. Bomans, C. Le Coadou, P. Fratzl, N.A.J.M. Sommerdijk, D. Faivre, *Nat. Mater.* **12**, 310 (2013)
17. D.S. Li, F. Soberanis, J. Fu, W.T. Hou, J.Z. Wu, D. Kisailus, *Cryst. Growth Des.* **13**, 422 (2013)
18. J.J. De Yoreo, P.U.P.A. Gilbert, N.A.J.M. Sommerdijk, R.L. Penn, S. Whitelam, D. Joester, H.Z. Zhang, J.D. Rimer, A. Navrotsky, J.F. Banfield, A.F. Wallace, F.M. Michel, F.C. Meldrum, H. Colfen, P.M. Dove, *Science* **349**, 6760 (2015)
19. M.L. Sushko, *J. Mater. Res.* **34**, 2914 (2019)
20. M.L. Sushko, *J. Cryst. Growth* **600**, 126914 (2022)
21. Y. Cheng, J. Tao, G. Zhu, J.A. Soltis, B.A. Legg, E. Nakouzi, J.J. De Yoreo, M.L. Sushko, J. Liu, *Nanoscale* **10**, 11907 (2018)
22. G.M. Zhu, M.L. Sushko, J.S. Loring, B.A. Legg, M. Song, J.A. Soltis, X.P. Huang, K.M. Rosso, J.J. De Yoreo, *Nature* **590**, 416 (2021)
23. L. Liu, E. Nakouzi, M.L. Sushko, G.K. Schenter, C.J. Mundy, J. Chun, J.J. De Yoreo, *Nat. Commun.* **11**, 1045 (2020)
24. Y.N. Wang, S.C. Xue, Q.Y. Lin, D. Song, Y. He, L.L. Liu, J.B. Zhou, M.R. Zong, J.J. De Yoreo, J.W. Zhu, K.M. Rosso, M.L. Sushko, X. Zang, *Proc. Natl. Acad. Sci. U.S.A.* **119**(11), e2112679119 (2022)
25. K.A. Fichthorn, *Chem. Eng. Sci.* **121**, 10 (2015)
26. M. Raju, A.C.T. van Duin, K.A. Fichthorn, *Nano Lett.* **14**, 1836 (2014)
27. N. Alcantar, J. Israelachvili, J. Boles, *Geochim. Cosmochim. Acta* **67**, 1289 (2003)
28. H.G. Liao, L.K. Cui, S. Whitelam, H.M. Zheng, *Science* **336**, 1011 (2012)
29. D.S. Li, M.H. Nielsen, J.R.I. Lee, C. Frandsen, J.F. Banfield, J.J. De Yoreo, *Science* **336**, 1014 (2012)
30. J. Israelachvili, *Intermolecular and Surface Forces* (Academic Press, New York, 1991)
31. N.D. Burrows, C.R.H. Hale, R.L. Penn, *Cryst. Growth Des.* **12**, 4787 (2012)
32. N.D. Burrows, C.R.H. Hale, R.L. Penn, *Cryst. Growth Des.* **13**, 3396 (2013)
33. R.L. Penn, J.A. Soltis, *CrystEngComm* **16**, 1409 (2014)
34. X.G. Xue, R.L. Penn, E.R. Leite, F. Huang, Z. Lin, *CrystEngComm* **16**, 1419 (2014)
35. S. Leikin, V.A. Parsegian, D.C. Rau, R.P. Rand, *Annu. Rev. Phys. Chem.* **44**, 369 (1993)
36. E. Schneck, F. Sedlmeier, R.R. Netz, *Proc. Natl. Acad. Sci. U.S.A.* **109**, 14405 (2012)
37. X. Zhang, Z. Shen, J. Liu, S.N. Kerisit, M.E. Bowden, M.L. Sushko, J.J. De Yoreo, K.M. Rosso, *Nat. Commun.* **8**, 835 (2017)
38. W.Q. Lv, W.D. He, X.N. Wang, Y.H. Niu, H.Q. Cao, J.H. Dickerson, Z.G. Wang, *Nanoscale* **6**, 2531 (2014)
39. Y.S. Leng, *Langmuir* **28**, 5339 (2012)
40. M.L. Sushko, K.M. Rosso, *Nanoscale* **8**, 19714 (2016)
41. J.C. Hopkins, R. Podgornik, W.Y. Ching, R.H. French, V.A. Parsegian, *J. Phys. Chem. C* **119**, 19083 (2015)
42. X. Zhang, Y. He, M.L. Sushko, J. Liu, L.L. Luo, J.J. De Yoreo, S.X. Mao, C.M. Wang, K.M. Rosso, *Science* **356**, 433 (2017)
43. D. Erts, A. Lohmus, R. Lohmus, H. Olin, A.V. Pokropivny, L. Ryen, K. Svensson, *Appl. Surf. Sci.* **188**, 460 (2002)
44. K. Yasui, K. Kato, *J. Phys. Chem. C* **119**, 24597 (2015)
45. G. Kresse, O. Dulub, U. Diebold, *Phys. Rev. B* **68**, 245409 (2003)
46. J.B.L. Martins, V. Moliner, J. Andres, E. Longo, C.A. Taft, *Theochem-J. Mol. Struct.* **330**, 347 (1995)
47. A. Onsten, D. Stoltz, P. Palmgren, S. Yu, M. Gothelid, U.O. Karlsson, *J. Phys. Chem. C* **114**, 11157 (2010)
48. J.A. Rodriguez, C.T. Campbell, *Surf. Sci.* **197**, 567 (1988)
49. M. Schiek, K. Al-Shamery, M. Kunat, F. Traeger, C. Woll, *Phys. Chem. Chem. Phys.* **8**, 1505 (2006)
50. R. Wahl, J.V. Lauritsen, F. Besenbacher, G. Kresse, *Phys. Rev. B* **87**, 085313 (2013)
51. H. Xu, L. Dong, X.Q. Shi, M.A. Van Hove, W.K. Ho, N. Lin, H.S. Wu, S.Y. Tong, *Phys. Rev. B* **89**, 235403 (2014)
52. H.G. Ye, G.D. Chen, H.B. Niu, Y.Z. Zhu, L. Shao, Z.J. Qiao, *J. Phys. Chem. C* **117**, 15976 (2013)
53. D. Mora-Fonz, T. Lazauskas, M.R. Farrow, C.R.A. Catlow, S.M. Woodley, A.A. Sokol, *Chem. Mater.* **29**, 5306 (2017)
54. C. Pacholski, A. Kornowski, H. Weller, *Angew. Chem. Int. Ed.* **41**(7), 1188 (2002)
55. B.L. Fan, Y.M. Zhang, R.L. Yan, J.Y. Fan, *CrystEngComm* **18**, 6492 (2016)
56. R.M. Pashley, J.N. Israelachvili, *J. Colloid Interface Sci.* **101**, 511 (1984)
57. D. Spagnoli, B. Gilbert, G.A. Waychunas, J.F. Banfield, *Geochim. Cosmochim. Acta* **73**, 4023 (2009)
58. H.Z. Zhang, J.J. De Yoreo, J.F. Banfield, *ACS Nano* **8**, 6526 (2014)
59 M. Bostrom, D.R.M. Williams, B.W. Ninham, *Phys. Rev. Lett.* **87**, 168103 (2001)
60. M. Dubois, T. Zemb, N. Fuller, R.P. Rand, V.A. Parsegian, *J. Chem. Phys.* **109**, 8731 (1998)
61. M. Dubois, T. Zemb, N. Fuller, R.P. Rand, V.A. Parsegian, *J. Chem. Phys.* **108**, 7855 (1998)
62. R.M. Pashley, P.M. McGuiggan, B.W. Ninham, J. Brady, D.F. Evans, *J. Phys. Chem.* **90**(8), 1637 (1986)
63. R.L. Penn, J.F. Banfield, *Am. Mineral.* **83**, 1077 (1998)
64. R.L. Penn, J.F. Banfield, *Geochim. Cosmochim. Acta* **63**, 1549 (1999)
65. P.M. McGuiggan, J.N. Israelachvili, *J. Mater. Res.* **5**, 2232 (1990)
66. P.M. McGuiggan, J.N. Israelachvili, *MRS Online Proc. Libr. Arch.* **138**, 349 (2011)
67. Q.Y. Tan, G.T. Zhao, Y.H. Qiu, Y.J. Kan, Z.H. Ni, Y.F. Chen, *Langmuir* **30**, 10845 (2014)
68. P.A. Pincus, S.A. Safran, *Europhys. Lett.* **42**, 103 (1998)
69. G.S. Manning, *Eur. Phys. J. E* **34**, 132 (2011)
70. K.S. Cho, D.V. Talapin, W. Gaschler, C.B. Murray, *J. Am. Chem. Soc.* **127**, 7140 (2005)
71. M.P. Boneschanscher, W.H. Evers, J.J. Geuchies, T. Altantzis, B. Goris, F.T. Rabouw, S.A.P. van Rossum, H.S.J. van der Zant, L.D.A. Siebbeles, G. Van Tendeloo, I. Swart, J. Hilhorst, A.V. Petukhov, S. Bals, D. Vanmaekelbergh, *Science* **344**, 1377 (2014)
72. U. Anand, J. Lu, D. Loh, Z. Aabdin, U. Mirsaidov, *Nano Lett.* **16**, 786 (2016)

73. K.-Y. Niu, H.-G. Liao, H. Zheng, *Microsc. Microanal.* **20**(2), 416 (2014)
74. Z. Aabdin, J. Lu, X. Zhu, U. Anand, N.D. Loh, H. Su, U. Mirsaidov, *Nano Lett.* **14**, 6639 (2014)
75. H.-G. Liao, H. Zheng, *J. Am. Chem. Soc.* **135**, 5038 (2013)
76. J.M. Yuk, J. Park, P. Ercius, K. Kim, D.J. Hellebusch, M.F. Crommie, J.Y. Lee, A. Zettl, A.P. Alivisatos, *Science* **336**, 61 (2012)
77. H. Zheng, R.K. Smith, Y.-W. Jun, C. Kisielowski, U. Dahmen, A.P. Alivisatos, *Science* **324**, 1309 (2009)
78. B. Jin, M.L. Sushko, Z.M. Liu, C.H. Jin, R.K. Tang, *Nano Lett.* **18**, 6551 (2018) □

Publisher's note
Springer Nature remains neutral with regard to jurisdictional claims in published maps and institutional affiliations.

Springer Nature or its licensor (e.g. a society or other partner) holds exclusive rights to this article under a publishing agreement with the author(s) or other rightsholder(s); author self-archiving of the accepted manuscript version of this article is solely governed by the terms of such publishing agreement and applicable law.

Maria L. Sushko is a computational scientist at the Pacific Northwest National Laboratory (PNNL). She received her PhD degree in physics from the Institute of Macromolecular Compounds RAS. She undertook her postgraduate research at Imperial College London and University College London, UK, before moving to PNNL. Her current work focuses on understanding interfacial processes that drive nucleation, growth, and assembly, and on developing a generalized modeling framework of crystallization that bridges atomic-scale dynamics and the formation and structure of mineral products at the mesoscale. Sushko can be reached by email at maria.sushko@pnnl.gov.